Digital Signal Processing ••• (••••) •••–•••

Contents lists available at ScienceDirect

Digital Signal Processing

www.elsevier.com/locate/dsp

A nested-PARAFAC based approach for target localization in bistatic MIMO radar systems

Paulo R.B. Gomes [a,*], André L.F. de Almeida [a], João Paulo C.L. da Costa [b], Rafael T. de Sousa Jr. [b]

[a] Federal University of Ceará, Department of Teleinformatics Engineering, Fortaleza, CE, Brazil
[b] University of Brasília, Department of Electrical Engineering, Brasília, DF, Brazil

ARTICLE INFO

Article history:
Available online xxxx

Keywords:
Target localization
DoD-DoA estimation
Multiple-input multiple-output (MIMO) radar
Nested-PARAFAC decomposition

ABSTRACT

Bistatic MIMO radar systems gather several advantages such as increased resilience to electronic countermeasures, unknown receiver location, higher identifiability of targets and direct application of several high resolution adaptive techniques. In this paper, we propose a tensor-based method for joint direction of departure (DoD) and direction of arrival (DoA) estimation in bistatic MIMO radar systems. By assuming that the transmit array is divided into two maximally overlapping subarrays, we initially model the cross-covariance matrix of the matched filters outputs as a Nested-PARAFAC decomposition of a fourth-order covariance tensor. Then, exploiting the structure of this decomposition, we first propose a two stage algorithm for joint DoD and DoA estimation of multiple targets based on double alternating least squares (DALS). In addition, for scenarios in which the number of receive antennas exceeds the number of targets, we propose a closed-form solution to the second stage of the proposed method based on the least squares Khatri-Rao factorization (LS-KRF) concept. Simulation results show that the proposed method offers a highly-accurate localization of multiple targets in real-world scenarios where the antenna elements at the transmit and receive arrays have positioning errors as well as less complexity compared to competing state-of-the-art tensor-based solutions.

1. Introduction

In recent years, research on target detection and localization techniques for multiple-input multiple-output (MIMO) radar systems has drawn great attention in the signal processing community [1–3]. In contrast to conventional phased-array radars that emits coherent waveforms, MIMO radar systems simultaneously transmit orthogonal waveforms using multiple antennas, increasing the performance of parameter estimation compared to previous ones [4]. Regarding the configuration of transmit and receive antennas, MIMO radars are divided in statistical [5] and colocated [6] MIMO radars. The former assumes that transmit and receive antennas are widely spaced, while the latter assumes antennas closely spaced, resulting in monostatic [7] or bistatic [8] MIMO radar schemes. Throughout this paper, we focus on the bistatic MIMO radar case, where the direction of departure (DoD) and direction of arrival (DoA) of the targets need to be jointly estimated.

Many techniques to solve the multiple targets localization problem in MIMO radar are based on traditional eigenspace algorithms, such as multiple signal classification (MUSIC) [9,10] and estimation of signal parameters via rotational invariance techniques (ESPRIT) [11,12]. However, MUSIC-based methods need a bidimensional search in the spatial spectrum to find the DoDs and DoAs of the targets. In this case, the accuracy of the estimated parameters is directly related to an increase in the computational cost. On the other hand, ESPRIT-based methods avoid the exhaustive peak search by exploiting the shift invariance property of the antenna array. However, this approach implies constraints on the geometry of the transmit and receive arrays, and a performance degradation is observed when the antenna elements have positioning errors. In [13], a direct-data tensor formulation based on the parallel factors (PARAFAC) decomposition [14,15] for joint DoD and DoD estimation in MIMO radar has been proposed. However, this approach becomes prohibitive when a large number of snapshots are processed at the receiver, motivating in this way, a tensor formulation based on second-order statistics which are long-term parameters that can be assumed to be constant over a larger time-scale. In addition, [13] also provides a performance analysis of tensor-based and matrix-based approaches, but it does not consider real-world

* Corresponding author.
E-mail addresses: paulo@gtel.ufc.br (P.R.B. Gomes), andre@gtel.ufc.br (A.L.F. de Almeida), joaopaulo.dacosta@ene.unb.br (J.P.C.L. da Costa), desousa@ene.unb.br (R.T. de Sousa).

https://doi.org/10.1016/j.dsp.2019.02.005
1051-2004/

scenarios where calibration errors are present at the transmit and receive arrays.

Recently, other strategies have also been proposed in the literature addressing target detection in MIMO radar applications. In [16], based on the generalized likelihood ratio test (GLRT) principle, the authors have derived F-test based detectors for target detection in passive multistatic radar scenarios. The authors of [17] have used a fourth-order cumulants based approach to formulate a sparse signal recovery problem in which the DoA estimation can be obtained in monostatic MIMO radar in the presence of gain-phase errors. Note that monostatic MIMO radar requires only the DoA estimation since the transmit and receive arrays are located closely, i.e., the DoD and DoA are equal. The work [18] explores the coprime array structure concept and its high number of degrees of freedom from the large virtual array aperture to achieve high resolution DoA estimation of mixed coherent and uncorrelated targets. In contrast to the aforementioned works, [19] consider unknown mutual coupling and a PARAFAC modeling is linked to the problem of joint DoD and DoA estimation for bistatic MIMO radar systems.

In this paper, we propose a tensor-based method for joint DoD and DoA estimation in bistatic MIMO radar systems. By assuming that the transmit array is divided into two maximally overlapping subarrays, we show that the cross-correlation matrix of the received signals after the matched filters can be modeled as a fourth-order tensor following a Nested-PARAFAC tensor decomposition [20]. Exploiting the multilinear structure of this decomposition, a two stage double alternating least squares (DALS) estimator is formulated from the inner and outer third-order PARAFAC parts of the Nested-PARAFAC model to solve the multi-target localization problem. In contrast to classical matrix-based and tensor-based ESPRIT versions [22,23], the proposed method does not impose any constraints on the geometry of the transmit and receive arrays. Moreover, it divides a high complexity fourth-order estimation problem into two third-order subproblems leading to a reduction in the processing time and complexity for parameter estimation when compared to state-of-the-art direct data [13] and covariance-based [24] solutions. Our simulation results also show that the proposed tensor-based receivers are capable of jointly estimating the spatial parameters of multiple targets with good accuracy even when the antenna arrays are vulnerable to calibration errors or have arbitrary geometries.

The Nested-PARAFAC decomposition has been successfully applied recently in the context of cooperative wireless communications systems. In [25] and [26], the authors proposed iterative and closed-form semi-blind receivers to jointly estimate the information symbols and the individual channels associated with the different communication links in one-way two-hop amplify-and-forward relaying schemes, respectively. Thereafter, [27] generalized this problem to the multihop relaying scenario by modeling the received signal at the destination as a generalized Nested-PARAFAC model. However, to the best of authors' knowledge this is the first work in the literature that links the Nested-PARAFAC decomposition to the target localization problem in bistatic MIMO radar systems.

The remainder of this paper is organized as follows. Section 2 provides a brief background on PARAFAC, Nested-PARAFAC and Tucker tensor decompositions. The material provided in this section also provides useful notations and definitions to be exploited later for the development of the proposed methods. In Section 3, the basic signal model for a bistatic MIMO radar system is presented. In Section 4, the cross-covariance tensor of the matched filters outputs for two transmit subarrays is modeled as a Nested-PARAFAC decomposition. Then, the two-stage tensor-based algorithm for joint DoD and DoA estimation is formulated. Uniqueness issues of the proposed Nested-PARAFAC based estimator are discussed in Section 5. In Section 6, the computational complexities of proposed and competing state-of-the-art algorithms are discussed. Simulation results are provided in Section 7 and the paper is concluded in Section 8.

Notation: Scalars are denoted by lower-case letters x, vectors as boldface lower-case letters $\boldsymbol{x}$, matrices as boldface upper-case letters $\boldsymbol{X}$ and tensors as boldface calligraphic letters $\boldsymbol{\mathcal{X}}$. The superscripts $\{\cdot\}^{\mathrm{T}}$, $\{\cdot\}^{*}$, $\{\cdot\}^{\mathrm{H}}$ and $\{\cdot\}^{\dagger}$ represent transpose, complex conjugate, conjugate transpose and pseudo-inverse operations. $E\{\cdot\}$ is the statistical expectation and $\|\cdot\|_{\mathrm{F}}$ represents the Frobenius norm of a matrix or tensor. The operator $\boldsymbol{X}(i,:)$ denotes the i-th row of $\boldsymbol{X} \in \mathbb{C}^{I\times J}$ while $\boldsymbol{X}(i:k,:)$, $i<k$, represents a submatrix formed by the i-th to j-th row of $\boldsymbol{X}$. $\boldsymbol{D}_i(\boldsymbol{X})$ denotes a diagonal matrix constructed from the i-th row of $\boldsymbol{X}$. $\circ$ denotes the outer product operator, $\otimes$ represents the Kronecker product and $\diamond$ is the Khatri-Rao product. The Khatri-Rao product between two matrices $\boldsymbol{X}=\left[\boldsymbol{x}_1,\ldots,\boldsymbol{x}_J\right]\in\mathbb{C}^{I\times J}$ and $\boldsymbol{Y}=\left[\boldsymbol{y}_1,\ldots,\boldsymbol{y}_J\right]\in\mathbb{C}^{K\times J}$ corresponds to a column-wise Kronecker product, i.e.:

$$\boldsymbol{X}\diamond\boldsymbol{Y}=\left[\boldsymbol{x}_1\otimes\boldsymbol{y}_1,\ldots,\boldsymbol{x}_J\otimes\boldsymbol{y}_J\right]\in\mathbb{C}^{IK\times J}. \tag{1}$$

Throughout this paper, the operations involving tensors are consistent with the definitions of [28].

2. Useful tensor decompositions

In order to facilitate the presentation of the proposed method, we first provide a brief overview on the PARAFAC, Nested-PARAFAC and Tucker tensor decompositions. These important models form the basis of our signal model and proposed tensor-based estimator that will be formulated in later sections of this paper.

2.1. PARAFAC decomposition

Using a third-order tensor formulation, the PARAlell FACtor Analysis (PARAFAC) decomposition [14,15] expresses a third-order tensor $\boldsymbol{\mathcal{X}}\in\mathbb{C}^{I_1\times I_2\times I_3}$ as a sum of R third-order rank-one tensors, i.e.,

$$\boldsymbol{\mathcal{X}}=\sum_{r=1}^{R}\boldsymbol{a}_r^{(1)}\circ\boldsymbol{a}_r^{(2)}\circ\boldsymbol{a}_r^{(3)}, \tag{2}$$

where R is known as the rank of the PARAFAC decomposition, i.e., is the minimum number of third-order rank-one tensors that are needed to reconstruct $\boldsymbol{\mathcal{X}}$ exactly. The vector $\boldsymbol{a}_r^{(n)}\in\mathbb{C}^{I_n}$ denotes the r-th column of the factor matrix $\boldsymbol{A}^{(n)}=\left[\boldsymbol{a}_1^{(n)},\cdots,\boldsymbol{a}_R^{(n)}\right]\mathbb{C}^{I_n\times R}$ along the n-th mode or dimension ($n=1,2,3$).

The PARAFAC decomposition (2) can be also represented in a more compact form by means of the n-mode product notation as follows [28]

$$\boldsymbol{\mathcal{X}}=\boldsymbol{\mathcal{I}}_{3,R}\times_1\boldsymbol{A}^{(1)}\times_2\boldsymbol{A}^{(2)}\times_3\boldsymbol{A}^{(3)}, \tag{3}$$

where the operator $\times_n$ ($n=1,2,3$) represents the n-mode product, while $\boldsymbol{\mathcal{I}}_{3,R}$ denotes a third-order identity tensor of size $R\times R\times R$. The elements of $\boldsymbol{\mathcal{I}}_{3,R}$ are equal to 1 when all indices are equal, and 0 elsewhere.

The tensor $\boldsymbol{\mathcal{X}}$ can also be written in three different ways using the "unfolding" concept, which consists in organizing its elements into a matrix form. In terms of the factor matrices $\boldsymbol{A}^{(1)}\in\mathbb{C}^{I_1\times R}$, $\boldsymbol{A}^{(2)}\in\mathbb{C}^{I_2\times R}$ and $\boldsymbol{A}^{(3)}\in\mathbb{C}^{I_3\times R}$, the unfolding matrices of $\boldsymbol{\mathcal{X}}$, defined as $[\boldsymbol{\mathcal{X}}]_{(1)}\in\mathbb{C}^{I_1\times I_2I_3}$, $[\boldsymbol{\mathcal{X}}]_{(2)}\in\mathbb{C}^{I_2\times I_1I_3}$ and $[\boldsymbol{\mathcal{X}}]_{(3)}\in\mathbb{C}^{I_3\times I_1I_2}$, admit the following factorizations [28]

$$[\boldsymbol{\mathcal{X}}]_{(1)}=\boldsymbol{A}^{(1)}\left(\boldsymbol{A}^{(3)}\diamond\boldsymbol{A}^{(2)}\right)^{\mathrm{T}}, \tag{4}$$

Please cite this article in press as: P.R.B. Gomes et al., A nested-PARAFAC based approach for target localization in bistatic MIMO radar systems, Digit. Signal Process. (2019), https://doi.org/10.1016/j.dsp.2019.02.005

$$[\mathcal{X}]_{(2)} = \boldsymbol{A}^{(2)} \left(\boldsymbol{A}^{(3)} \diamond \boldsymbol{A}^{(1)} \right)^{\mathrm{T}}, \tag{5}$$

$$[\mathcal{X}]_{(3)} = \boldsymbol{A}^{(3)} \left(\boldsymbol{A}^{(2)} \diamond \boldsymbol{A}^{(1)} \right)^{\mathrm{T}}, \tag{6}$$

where the operator $\diamond$ denotes the Khatri-Rao product (i.e., column-wise Kronecker product).

2.2. Nested-PARAFAC decomposition

The Nested-PARAFAC decomposition introduced by [20] assumes that the n-th factor matrix $\boldsymbol{A}^{(n)} \in \mathbb{C}^{I_n \times R}$ in (3) is itself an unfolding of an additional PARAFAC decomposition (see [20] for further details). For simplicity, let $\boldsymbol{A}^{(1)} \in \mathbb{C}^{I_1 \times R}$ denote the 1-mode unfolding of $\mathcal{Y} \in \mathbb{C}^{J_1 \times J_2 \times J_3}$, i.e., $\boldsymbol{A}^{(1)} = [\mathcal{Y}]_{(1)}$ in which $J_1 = I_1$ and $J_2 J_3 = R$. From this assumption, we can define the Nested-PARAFAC decomposition of $\mathcal{X}$ in terms of the following two (linked) PARAFAC decompositions

$$\mathcal{X} = \mathcal{I}_{3,R} \times_1 [\mathcal{Y}]_{(1)} \times_2 \boldsymbol{A}^{(2)} \times_3 \boldsymbol{A}^{(3)}, \tag{7}$$

$$\mathcal{Y} = \mathcal{I}_{3,Q} \times_1 \boldsymbol{B}^{(1)} \times_2 \boldsymbol{B}^{(2)} \times_3 \boldsymbol{B}^{(3)}, \tag{8}$$

where (7) is called outer PARAFAC part, while (8) is called inner PARAFAC part of rank Q [21]. $\boldsymbol{B}^{(1)} \in \mathbb{C}^{J_1 \times Q}$, $\boldsymbol{B}^{(2)} \in \mathbb{C}^{J_2 \times Q}$ and $\boldsymbol{B}^{(3)} \in \mathbb{C}^{J_3 \times Q}$ are the factor matrices of the inner PARAFAC part.

2.3. Fourth-order Tucker decomposition

The fourth-order Tucker decomposition factorizes $\mathcal{X} \in \mathbb{C}^{I_1 \times I_2 \times I_3 \times I_4}$ as a multilinear transformation of a fourth-order core tensor $\mathcal{G} \in \mathbb{C}^{R_1 \times R_2 \times R_3 \times R_4}$ by the factor matrices $\boldsymbol{A}^{(n)} \in \mathbb{C}^{I_n \times R_n}$ along the tensor modes ($n = 1, 2, 3, 4$). The value R_n denotes the rank of the decomposition along the n-th mode ($n = 1, 2, 3, 4$), while the set (R_1, R_2, R_3, R_4) is called multilinear rank of $\mathcal{X}$ [29]. Using the n-mode product notation, the fourth-order Tucker decomposition can be written as

$$\mathcal{X} = \mathcal{G} \times_1 \boldsymbol{A}^{(1)} \times_2 \boldsymbol{A}^{(2)} \times_3 \boldsymbol{A}^{(3)} \times_4 \boldsymbol{A}^{(4)}. \tag{9}$$

In general, the Tucker decomposition does not impose constraints on the structure of the core tensor $\mathcal{G}$. On the other hand, the PARAFAC decomposition can be viewed as a special case of the Tucker decomposition in which $\mathcal{G}$ is an identity tensor and $R_n = R$ ($n = 1, 2, 3, 4$).

3. Signal model

We consider a narrowband bistatic MIMO radar system in which the transmit and receive arrays have M and N antenna elements, respectively. At the transmit side, each antenna element emits one waveform. The M transmitted waveforms have identical bandwidth and center frequency but are temporally orthogonal. The waveform vector transmitted by the m-th array element within one repetition interval is denoted by $\boldsymbol{s}_m \in \mathbb{C}^{1 \times K}$, $m = 1, \ldots, M$, where K is the number of samples per pulse period and $\boldsymbol{s}_m \boldsymbol{s}_m^{\mathrm{H}} = K$. We also assume that P targets in the far-field of the transmit and receive arrays, with different Doppler frequencies located at the same range bin of interest. The location of the p-th target, $p = 1, \ldots, P$, is denoted by (ϕ_p, θ_p), where ϕ_p and θ_p are the DoD and DoA with respect to the transmit and receive arrays, respectively. The received signal $\boldsymbol{X}^{(l)} \in \mathbb{C}^{N \times K}$ at the output of the receive array in the l-th pulse period, $l = 1, \ldots, L$, from reflections of P targets is given by [11]

$$\boldsymbol{X}^{(l)} = \sum_{p=1}^{P} \boldsymbol{a}_{\mathrm{r}}(\theta_p) \beta_p^{(l)} \boldsymbol{a}_{\mathrm{t}}^{\mathrm{T}}(\phi_p) \begin{bmatrix} \boldsymbol{s}_1 \\ \vdots \\ \boldsymbol{s}_M \end{bmatrix} e^{j2\pi f_{\mathrm{D}p} t_l} + \boldsymbol{N}^{(l)}, \quad l = 1, \ldots, L \tag{10}$$

where $\beta_p^{(l)}$ denotes the complex-valued reflection coefficient of the p-th target assumed constant during a pulse period, $f_{\mathrm{D}p}$ is the Doppler frequency of the p-th target, t_l is the slow time index of the l-th pulse period and $\boldsymbol{N}^{(l)} \in \mathbb{C}^{N \times K}$ denotes the additive white Gaussian noise (AWGN) contribution.

The steering vectors of the transmit and receive arrays with respect to the p-th target, $\boldsymbol{a}_{\mathrm{t}}(\phi_p) \mathbb{C}^{M \times 1}$ and $\boldsymbol{a}_{\mathrm{r}}(\theta_p) \in \mathbb{C}^{N \times 1}$, assume arbitrary geometries, and are computed as functions of the angular parameters ϕ_p and θ_p, respectively. For instance, considering a linear array with positioning errors between the antenna elements, the m-th and n-th entries of $\boldsymbol{a}_{\mathrm{t}}(\phi_p)$ and $\boldsymbol{a}_{\mathrm{r}}(\theta_p)$ are modeled as $[\boldsymbol{a}_{\mathrm{t}}(\phi_p)]_m = e^{j\frac{2\pi}{\lambda}[(m-1)d_t + \alpha\epsilon_m]\sin\phi_p}$ and $[\boldsymbol{a}_{\mathrm{r}}(\theta_p)]_n = e^{j\frac{2\pi}{\lambda}[(n-1)d_r + \alpha\epsilon_n]\sin\theta_p}$, where λ denotes the wavelength of the transmitted signal, d_t and d_r are the inter-element spacing of the transmit and receive arrays, α denotes a positioning error factor, while ϵ_m and ϵ_n are zero mean real Gaussian random variables assumed different for each value of $m = 1, \ldots, M$ and $n = 1 \ldots, N$. In contrast to real-world scenarios in which positioning errors are present in both transmit and receive arrays, the ESPRIT-based algorithms [22,23] assume antenna arrays that satisfy the shift invariance property and have good accuracy (only valid in the ideal case, when $\alpha \to 0$).

Due to the orthogonality of the transmitted waveforms, the received signal (10) can be matched to the m-th waveform $\boldsymbol{s}_m$, $m = 1, \ldots, M$. The output of the matched filters w.r.t. the m-th transmitted waveform is given by

$$\boldsymbol{y}_m^{(l)} = \frac{1}{K} \boldsymbol{X}^{(l)} \boldsymbol{s}_m^{\mathrm{H}} = \boldsymbol{A}_{\mathrm{r}} \boldsymbol{D}_m(\boldsymbol{A}_{\mathrm{t}}) \boldsymbol{\gamma}^{(l)} + \boldsymbol{w}_m^{(l)} \in \mathbb{C}^{N \times 1}, \tag{11}$$

where $\boldsymbol{A}_{\mathrm{t}} = [\boldsymbol{a}_{\mathrm{t}}(\phi_1), \ldots, \boldsymbol{a}_{\mathrm{t}}(\phi_P)] \in \mathbb{C}^{M \times P}$ denotes the transmit steering matrix, $\boldsymbol{A}_{\mathrm{r}} = [\boldsymbol{a}_{\mathrm{r}}(\theta_1), \ldots, \boldsymbol{a}_{\mathrm{r}}(\theta_P)] \in \mathbb{C}^{N \times P}$ is the receive steering matrix, $\boldsymbol{\gamma}^{(l)} = \left[\beta_1^{(l)} e^{j2\pi f_{\mathrm{D}1} t_l}, \ldots, \beta_P^{(l)} e^{j2\pi f_{\mathrm{D}P} t_l} \right]^{\mathrm{T}} \in \mathbb{C}^{P \times 1}$ and $\boldsymbol{w}_m^{(l)} = \frac{1}{K} \boldsymbol{N}^{(l)} \boldsymbol{s}_m^{\mathrm{H}} \in \mathbb{C}^{N \times 1}$ is the noise contribution at the matched filter output associated with the m-th transmitted waveform.

Our aim is to locate the P targets in the same range bin of interest by estimating their DoDs and DoAs. In the following, by starting from the output signals of the matched filters in (11), we formulate the proposed two-stage tensor-based method for the joint estimation of the spatial target parameters.

4. Proposed tensor-based method for joint DoD and DoA estimation

Let us consider that the transmit array is divided into two smaller subarrays. We assume maximally overlapping subarrays, i.e., the first subarray contains the first $M - 1$ antenna elements of the transmit array, while the second subarray contains its last $M - 1$ antenna elements. The received signal at the output of the matched filters associated with the first subarray is given by

$$\boldsymbol{z}_1^{(l)} = \begin{bmatrix} \boldsymbol{y}_1^{(l)} \\ \vdots \\ \boldsymbol{y}_{M-1}^{(l)} \end{bmatrix} = \begin{bmatrix} \boldsymbol{A}_{\mathrm{r}} \boldsymbol{D}_1(\boldsymbol{A}_{\mathrm{t}}) \boldsymbol{\gamma}^{(l)} \\ \vdots \\ \boldsymbol{A}_{\mathrm{r}} \boldsymbol{D}_{M-1}(\boldsymbol{A}_{\mathrm{t}}) \boldsymbol{\gamma}^{(l)} \end{bmatrix} + \begin{bmatrix} \boldsymbol{w}_1^{(l)} \\ \vdots \\ \boldsymbol{w}_{M-1}^{(l)} \end{bmatrix} = \left(\boldsymbol{A}_{\mathrm{t},1} \diamond \boldsymbol{A}_{\mathrm{r}} \right) \boldsymbol{\gamma}^{(l)} + \boldsymbol{w}_{\mathrm{MF1}}^{(l)} \in \mathbb{C}^{(M-1)N \times 1}, \tag{12}$$

where $\boldsymbol{A}_{\mathrm{t},1} = [\boldsymbol{a}_{\mathrm{t},1}(\phi_1), \ldots, \boldsymbol{a}_{\mathrm{t},1}(\phi_P)] \in \mathbb{C}^{(M-1) \times P}$ denotes the transmit steering matrix of the first subarray. In a similar way, the

output signals associated with the second subarray can be written as

$$\boldsymbol{z}_2^{(l)} = \begin{bmatrix} \boldsymbol{y}_2^{(l)} \\ \vdots \\ \boldsymbol{y}_M^{(l)} \end{bmatrix} = \begin{bmatrix} \boldsymbol{A}_{\mathrm{r}} \boldsymbol{D}_2\left(\boldsymbol{A}_{\mathrm{t}}\right) \boldsymbol{\gamma}^{(l)} \\ \vdots \\ \boldsymbol{A}_{\mathrm{r}} \boldsymbol{D}_M\left(\boldsymbol{A}_{\mathrm{t}}\right) \boldsymbol{\gamma}^{(l)} \end{bmatrix} + \begin{bmatrix} \boldsymbol{w}_2^{(l)} \\ \vdots \\ \boldsymbol{w}_M^{(l)} \end{bmatrix} = \left(\boldsymbol{A}_{\mathrm{t},2} \diamond \boldsymbol{A}_{\mathrm{r}}\right) \boldsymbol{\gamma}^{(l)} + \boldsymbol{w}_{\mathrm{MF2}}^{(l)} \in \mathbb{C}^{(M-1)N\times 1}, \tag{13}$$

where $\boldsymbol{A}_{\mathrm{t},2} = [\boldsymbol{a}_{\mathrm{t},2}(\phi_1), \ldots, \boldsymbol{a}_{\mathrm{t},2}(\phi_P)] \in \mathbb{C}^{(M-1)\times P}$ denotes the transmit steering matrix of the second subarray. The vector $\boldsymbol{w}_{\mathrm{MF}i}^{(l)} \in \mathbb{C}^{(M-1)N\times 1}$ is the noise term at the matched filter output with respect to the i-th transmit subarray ($i = 1, 2$).

From (12) and (13), the cross-covariance matrix $\boldsymbol{R} \in \mathbb{C}^{(M-1)N\times(M-1)N}$ between the subarrays output signals is given by

$$\begin{aligned} \boldsymbol{R} &= E\left\{\boldsymbol{z}_2^{(l)} \boldsymbol{z}_1^{(l)\mathrm{H}}\right\}, \quad l = 1, \ldots, L \\ &= \left(\boldsymbol{A}_{\mathrm{t},2} \diamond \boldsymbol{A}_{\mathrm{r}}\right) \boldsymbol{R}_{\gamma} \left(\boldsymbol{A}_{\mathrm{t},1} \diamond \boldsymbol{A}_{\mathrm{r}}\right)^{\mathrm{H}} + \boldsymbol{R}_w, \end{aligned} \tag{14}$$

where $\boldsymbol{R}_{\gamma} = E\left\{\boldsymbol{\gamma}^{(l)} \boldsymbol{\gamma}^{(l)\mathrm{H}}\right\} \in \mathbb{C}^{P\times P}$. The term $\boldsymbol{R}_w = E\left\{\boldsymbol{w}_{\mathrm{MF2}}^{(l)} \boldsymbol{w}_{\mathrm{MF1}}^{(l)\mathrm{H}}\right\} \in \mathbb{C}^{(M-1)N\times(M-1)N}$ denotes the unknown noise contribution.

Note that the cross-covariance matrix $\boldsymbol{R}$ in (14) can be viewed as a multimode unfolding of the following fourth-order cross-covariance tensor $\boldsymbol{\mathcal{R}} \in \mathbb{C}^{N\times(M-1)\times N\times(M-1)}$

$$\boldsymbol{\mathcal{R}} = \boldsymbol{\mathcal{R}}_{\gamma} \times_1 \boldsymbol{A}_{\mathrm{r}} \times_2 \boldsymbol{A}_{\mathrm{t},2} \times_3 \boldsymbol{A}_{\mathrm{r}}^{*} \times_4 \boldsymbol{A}_{\mathrm{t},1}^{*} + \boldsymbol{\mathcal{R}}_w, \tag{15}$$

where $\boldsymbol{\mathcal{R}}_{\gamma} \in \mathbb{C}^{P\times P\times P\times P}$ and $\boldsymbol{\mathcal{R}}_w \in \mathbb{C}^{N\times(M-1)\times N\times(M-1)}$ are obtained by "tensorizing" $\boldsymbol{R}_{\gamma}$ and $\boldsymbol{R}_w$ as fourth-order tensors of sizes $P \times P \times P \times P$ and $N \times (M-1) \times N \times (M-1)$, respectively. Indeed, the noiseless part of (15) satisfies a fourth-order Tucker decomposition. By comparing (15) with (9), the following correspondences can be deduced

$$\left(I_1, I_2, I_3, I_4, R_{n=1,2,3,4}\right) \leftrightarrow (N, (M-1), N, (M-1), P),$$

$$\left(\mathcal{G}, \boldsymbol{A}^{(1)}, \boldsymbol{A}^{(2)}, \boldsymbol{A}^{(3)}, \boldsymbol{A}^{(4)}\right) \leftrightarrow \left(\boldsymbol{\mathcal{R}}_{\gamma}, \boldsymbol{A}_r, \boldsymbol{A}_{t,2}, \boldsymbol{A}_r^{*}, \boldsymbol{A}_{t,1}^{*}\right).$$

The estimation of the targets' spatial parameters (DoDs and DoAs) can be obtained using different approaches such as ESPRIT-based algorithms [22,23], PARAFAC-based direct-data algorithms [13], and ALS-Tucker4 algorithms [24]. The first approach [22, 23] assumes perfect array calibration. Array imperfections in real-world scenarios may severely degrade the estimation accuracy of these methods. In addition, although the direct-data algorithm of [13] provide good estimation accuracy by applying a PARAFAC-based algorithm directly to the received data tensor, the computational complexity of the tensor-based estimator may be high when the data block size is large. In the ALS-Tucker4 algorithm proposed in [24], five LS estimation steps are necessary to estimate the factor matrices and the core tensor from the cross-correlation tensor (15). However, this approach also has a high computational cost and may present slow convergence due the wide search space to alternately minimize a cost function with five unknown matrices, represented by the core tensor and four factor matrices that model the covariance tensor. In the following, we formulate a new algorithm for joint DoD and DoA estimation that is based on a two-stage Nested-PARAFAC modeling approach. As will be clear in the sequel, the Nested-PARAFAC approach breaks down the complex fourth-order tensor problem (15) into two smaller third-order tensor subproblems, without affecting the accuracy of the parameter estimation.

4.1. Proposed nested-PARAFAC based estimator

The cross-covariance matrix $\boldsymbol{R}$ in (14) can now be viewed as an unfolding matrix of a third-order cross-covariance tensor $\boldsymbol{\mathcal{R}} \in \mathbb{C}^{(M-1)N\times N\times(M-1)}$ expressed in n-mode product notation as

$$\boldsymbol{\mathcal{R}} = \mathcal{I}_{3,P} \times_1 [\boldsymbol{\mathcal{A}}]_{(1)}^{\mathrm{T}} \times_2 \boldsymbol{A}_{\mathrm{r}}^{*} \times_3 \boldsymbol{A}_{\mathrm{t},1}^{*} + \boldsymbol{\mathcal{R}}_w, \tag{16}$$

where $\boldsymbol{\mathcal{R}}_w \in \mathbb{C}^{(M-1)N\times N\times(M-1)}$ is now a third-order cross-covariance noise tensor. The factor matrix $[\boldsymbol{\mathcal{A}}]_{(1)}^{\mathrm{T}} \in \mathbb{C}^{(M-1)N\times P}$ in (16) denotes the transpose of the 1-mode unfolding of the following third-order PARAFAC decomposition

$$\boldsymbol{\mathcal{A}} = \mathcal{I}_{3,P} \times_1 \boldsymbol{R}_{\gamma}^{\mathrm{T}} \times_2 \boldsymbol{A}_{\mathrm{r}} \times_3 \boldsymbol{A}_{\mathrm{t},2}. \tag{17}$$

The noiseless term of the cross-covariance tensor (16) corresponds to the Nested-PARAFAC decomposition [20] of a fourth-order tensor. By analogy with (7) and (8), we can deduce the following correspondences

$$\underbrace{\left(\boldsymbol{\mathcal{X}}, [\boldsymbol{\mathcal{Y}}]_{(1)}, \boldsymbol{A}^{(2)}, \boldsymbol{A}^{(3)}\right) \leftrightarrow \left(\boldsymbol{\mathcal{R}}, [\boldsymbol{\mathcal{A}}]_{(1)}^{\mathrm{T}}, \boldsymbol{A}_r^{*}, \boldsymbol{A}_{t,1}^{*}\right)}_{\text{outer PARAFAC part}},$$

$$\underbrace{\left(\boldsymbol{\mathcal{Y}}, \boldsymbol{B}^{(1)}, \boldsymbol{B}^{(2)}, \boldsymbol{B}^{(3)}\right) \leftrightarrow \left(\boldsymbol{\mathcal{A}}, \boldsymbol{R}_{\gamma}^{\mathrm{T}}, \boldsymbol{A}_r, \boldsymbol{A}_{t,2}\right)}_{\text{inner PARAFAC part}}.$$

4.2. First ALS stage (trilinear ALS)

In accordance with (4), (5) and (6), the outer PARAFAC part (16) admits the following representations in terms of its 1-mode, 2-mode and 3-mode unfolding matrices

$$[\boldsymbol{\mathcal{R}}]_{(1)} = [\boldsymbol{\mathcal{A}}]_{(1)}^{\mathrm{T}} \left(\boldsymbol{A}_{\mathrm{t},1}^{*} \diamond \boldsymbol{A}_{\mathrm{r}}^{*}\right)^{\mathrm{T}} + [\boldsymbol{\mathcal{R}}_w]_{(1)}, \tag{18}$$

$$[\boldsymbol{\mathcal{R}}]_{(2)} = \boldsymbol{A}_{\mathrm{r}}^{*} \left(\boldsymbol{A}_{\mathrm{t},1}^{*} \diamond [\boldsymbol{\mathcal{A}}]_{(1)}^{\mathrm{T}}\right)^{\mathrm{T}} + [\boldsymbol{\mathcal{R}}_w]_{(2)}, \tag{19}$$

$$[\boldsymbol{\mathcal{R}}]_{(3)} = \boldsymbol{A}_{\mathrm{t},1}^{*} \left(\boldsymbol{A}_{\mathrm{r}}^{*} \diamond [\boldsymbol{\mathcal{A}}]_{(1)}^{\mathrm{T}}\right)^{\mathrm{T}} + [\boldsymbol{\mathcal{R}}_w]_{(3)}. \tag{20}$$

Assuming that the number of targets is known or has been previously estimated using, e.g., the methods proposed in [30,31], estimates of the factor matrices $[\boldsymbol{\mathcal{A}}]_{(1)}^{\mathrm{T}}$, $\boldsymbol{A}_{\mathrm{r}}^{*}$ and $\boldsymbol{A}_{\mathrm{t},1}^{*}$ can be obtained from the outer PARAFAC part using the alternating least squares (ALS) algorithm [32]. The first trilinear ALS stage of the proposed method consists of estimating the matrices of interest in an alternating way from the unfolding matrices $[\boldsymbol{\mathcal{R}}]_{(n=1,2,3)}$ by solving three linear LS problems from (18), (19) and (20), whose analytic solutions are given by $[\hat{\boldsymbol{\mathcal{A}}}]_{(1)}^{\mathrm{T}} = [\boldsymbol{\mathcal{R}}]_{(1)} \left[\left(\boldsymbol{A}_{\mathrm{t},1}^{*} \diamond \boldsymbol{A}_{\mathrm{r}}^{*}\right)^{\mathrm{T}}\right]^{\dagger}$, $\hat{\boldsymbol{A}}_{\mathrm{r}}^{*} = [\boldsymbol{\mathcal{R}}]_{(2)} \left[\left(\boldsymbol{A}_{\mathrm{t},1}^{*} \diamond [\boldsymbol{\mathcal{A}}]_{(1)}^{\mathrm{T}}\right)^{\mathrm{T}}\right]^{\dagger}$ and $\hat{\boldsymbol{A}}_{\mathrm{t},1}^{*} = [\boldsymbol{\mathcal{R}}]_{(3)} \left[\left(\boldsymbol{A}_{\mathrm{r}}^{*} \diamond [\boldsymbol{\mathcal{A}}]_{(1)}^{\mathrm{T}}\right)^{\mathrm{T}}\right]^{\dagger}$, respectively.

Each iteration of the first trilinear ALS stage contains three LS estimation steps to update $[\hat{\boldsymbol{\mathcal{A}}}]_{(1)}^{\mathrm{T}}$, $\hat{\boldsymbol{A}}_{\mathrm{r}}^{*}$ and $\hat{\boldsymbol{A}}_{\mathrm{t},1}^{*}$ in an iterative way. At each step, a given factor matrix is updated by fixing the other two to their estimates obtained at previous updating steps. This procedure is repeated until the convergence of the first stage. Convergence of the first trilinear ALS stage at the i-th iteration is declared when $|e_{(i)} - e_{(i-1)}| \leq 10^{-6}$, where $e_{(i)}$ denotes the residual error at the i-th iteration defined as

$$e_{(i)} = \left\| \boldsymbol{\mathcal{R}} - \hat{\boldsymbol{\mathcal{R}}}_{(i)} \right\|_{\mathrm{F}}^{2}, \tag{21}$$

where $\hat{\boldsymbol{\mathcal{R}}}_{(i)}$ is the reconstructed version of the cross-covariance tensor obtained from the estimated factor matrices at the end of the i-th iteration.

Please cite this article in press as: P.R.B. Gomes et al., A nested-PARAFAC based approach for target localization in bistatic MIMO radar systems, Digit. Signal Process. (2019), https://doi.org/10.1016/j.dsp.2019.02.005

4.3. Second ALS stage (bilinear ALS)

After the convergence of the first (trilinear) ALS stage, a second (bilinear) ALS stage can be formulated to estimate the factor matrices $\boldsymbol{A}_{t,2}$ and $\boldsymbol{R}_\gamma$ from the outputs $\hat{\boldsymbol{A}}_r$ and $[\hat{\boldsymbol{\mathcal{A}}}]_{(1)}$ of the first stage. Thanks to the Nested-PARAFAC structure of $\boldsymbol{\mathcal{R}}$, the estimated factor matrix $[\hat{\boldsymbol{\mathcal{A}}}]_{(1)}$ can be recast as a third-order PARAFAC decomposition in unfolded form. Thus, in a similar way, and assuming now that $\hat{\boldsymbol{A}}_r$ is fixed in the second stage, the matrices of interest can be obtained from the unfolding matrices

$$[\boldsymbol{\mathcal{A}}]_{(1)} = \boldsymbol{R}_\gamma^{\mathrm{T}} \left(\boldsymbol{A}_{t,2} \diamond \boldsymbol{A}_r\right)^{\mathrm{T}} \tag{22}$$

$$[\boldsymbol{\mathcal{A}}]_{(3)} = \boldsymbol{A}_{t,2}^{\mathrm{T}} \left(\boldsymbol{A}_r \diamond \boldsymbol{R}_\gamma^{\mathrm{T}}\right)^{\mathrm{T}} \tag{23}$$

by solving two linear LS problems whose analytic solutions are given by $\hat{\boldsymbol{R}}_\gamma^{\mathrm{T}} = [\boldsymbol{\mathcal{A}}]_{(1)} \left[\left(\boldsymbol{A}_{t,2} \diamond \boldsymbol{A}_r\right)^{\mathrm{T}}\right]^{\dagger}$ and $\hat{\boldsymbol{A}}_{t,2} = [\boldsymbol{\mathcal{A}}]_{(3)} \times \left[\left(\boldsymbol{A}_r \diamond \boldsymbol{R}_\gamma^{\mathrm{T}}\right)\right]^{\dagger}$, respectively. Note that, this second ALS stage has a faster convergence since it estimates only two factor matrices due to the knowledge of $\boldsymbol{A}_r$ obtained previously in the first ALS stage.

4.4. Estimation of DoD and DoA parameters

By exploiting the redundancy inserted by the maximally overlapping subarrays, a final estimate of the transmit steering matrix is computed from $\hat{\boldsymbol{A}}_{\mathrm{t},1}$ obtained in the trilinear ALS stage and from $\hat{\boldsymbol{A}}_{\mathrm{t},2}$ obtained in the bilinear ALS stage using the following relation:

$$\hat{\boldsymbol{A}}_{\mathrm{t}} = \begin{bmatrix} \hat{\boldsymbol{A}}_{\mathrm{t},1}\,(1,:) \\ \frac{1}{2}\left[\hat{\boldsymbol{A}}_{\mathrm{t},1}\,(2:M-1,:) + \hat{\boldsymbol{A}}_{\mathrm{t},2}\,(1:M-2,:)\right] \\ \hat{\boldsymbol{A}}_{\mathrm{t},2}\,(M-1,:) \end{bmatrix}. \tag{24}$$

The final step of the proposed method is to estimate the DoDs and DoAs of P targets. For the p-th target, which corresponds to the p-th column of the estimated transmit and receive steering matrices, estimates of its angular parameters $\hat{\phi}_p$ and $\hat{\theta}_p$ can be obtained from a one-dimensional peak search in the following spatial spectra [33]:

$$\hat{\phi}_p = \underset{\phi_p}{\operatorname{argmax}} \left|\boldsymbol{a}_{\mathrm{t}}^{\mathrm{H}}(\phi_p) \cdot \hat{\boldsymbol{a}}_{\mathrm{t}}(\hat{\phi}_p)\right|, \tag{25}$$

$$\hat{\theta}_p = \underset{\theta_p}{\operatorname{argmax}} \left|\boldsymbol{a}_{\mathrm{r}}^{\mathrm{H}}(\theta_p) \cdot \hat{\boldsymbol{a}}_{\mathrm{r}}(\hat{\theta}_p)\right|, \tag{26}$$

where $\boldsymbol{a}_{\mathrm{t}}(\phi_p)$ and $\boldsymbol{a}_{\mathrm{r}}(\theta_p)$ are the known array monifolds of the transmit and receive arrays for a given angle pair (ϕ_p, θ_p), respectively.

The proposed tensor-based double alternating least squares (DALS) algorithm for multi-target localization is summarized in Algorithm 1.

4.5. Alternative closed-form solution to the second stage

When $N \geq P$ an estimate to $\boldsymbol{A}_{\mathrm{t},2}$ can be obtained from the first stage output $[\hat{\boldsymbol{\mathcal{A}}}]_{(1)}$ in closed-form by means of the least squares Khatri-Rao factorization (LS-KRF) algorithm [34]. Multiplying both sides of $[\hat{\boldsymbol{\mathcal{A}}}]_{(2)}^{\mathrm{T}}$ by the pseudo-inverse of $\hat{\boldsymbol{A}}_{\mathrm{r}}^{\mathrm{T}}$ obtained in the first step, the p-th column of the resulting matrix $\hat{\boldsymbol{A}}_{\mathrm{t},2} \diamond \hat{\boldsymbol{R}}_\gamma^{\mathrm{T}}$ denotes the vectorization operation of the rank-one matrix $\boldsymbol{\Psi}_p = \boldsymbol{r}_p^* \circ \boldsymbol{a}_{\mathrm{t},2}(\phi_p) \in \mathbb{C}^{P\times(M-1)}$, where $\boldsymbol{r}_p \in \mathbb{C}^{P\times 1}$ is the p-th column of the covariance matrix $\hat{\boldsymbol{R}}_\gamma$. Defining $\boldsymbol{U}_p \boldsymbol{\Sigma}_p \boldsymbol{V}_p^{\mathrm{H}}$ as the singular value decomposition (SVD) of $\boldsymbol{\Psi}_p$, estimates of $\boldsymbol{r}_p^*$ and $\boldsymbol{a}_{\mathrm{t},2}(\phi_p)$, $p = 1, \ldots, P$, can be obtained by truncating the SVD to a rank-one approximation as follows [34]:

$$\hat{\boldsymbol{r}}_p^* = \sqrt{\sigma_1}\boldsymbol{u}_1 \quad \text{and} \quad \hat{\boldsymbol{a}}_{\mathrm{t},2}(\phi_p) = \sqrt{\sigma_1}\boldsymbol{v}_1^*, \tag{27}$$

where $\boldsymbol{u}_1 \in \mathbb{C}^{P\times 1}$ and $\boldsymbol{v}_1 \in \mathbb{C}^{(M-1)\times 1}$ are the first left and right singular vectors of $\boldsymbol{U}_p$ and $\boldsymbol{V}_p$, respectively, and σ_1 is the largest singular value. The estimates of the matrices $\hat{\boldsymbol{A}}_{\mathrm{t},2}$ and $\hat{\boldsymbol{R}}_\gamma$ are obtained by repeating this procedure for $p = 1, \ldots, P$.

Remark: Note that the LS-KRF and peak search steps can be computed independently for each column of the estimated matrices. Thus, the estimates of DoDs and DoAs can be obtained in a parallel way if P processors are available, reducing the processing time by a factor of P. A version of the proposed tensor-based algorithm using the closed-form LS-KRF solution in the second stage is summarized in Algorithm 2.

Algorithm 1: Proposed DALS algorithm for joint DoD and DoA estimation.

- **Trilinear ALS Stage:**

(1.1) *Set* $i = 0$ *and initialize randomly* $\hat{\boldsymbol{A}}_{\mathrm{t},1(i=0)}$ *and* $\hat{\boldsymbol{A}}_{\mathrm{r}(i=0)}$;
(1.2) $i = i + 1$;
(1.3) *From* $[\boldsymbol{\mathcal{R}}]_{(1)}$, *obtain an LS estimate of* $[\boldsymbol{\mathcal{A}}]_{(1)}$:
$[\hat{\boldsymbol{\mathcal{A}}}]_{(1)(i)}^{\mathrm{T}} = [\boldsymbol{\mathcal{R}}]_{(1)} \left[\left(\hat{\boldsymbol{A}}_{\mathrm{t},1(i-1)} \diamond \hat{\boldsymbol{A}}_{\mathrm{r}(i-1)}\right)^{\mathrm{H}}\right]^{\dagger}$;
(1.4) *From* $[\boldsymbol{\mathcal{R}}]_{(2)}$, *obtain an LS estimate of* $\boldsymbol{A}_{\mathrm{r}}^*$:
$\hat{\boldsymbol{A}}_{\mathrm{r}(i)}^* = [\boldsymbol{\mathcal{R}}]_{(2)} \left[\left(\boldsymbol{A}_{\mathrm{t},1(i-1)}^* \diamond [\hat{\boldsymbol{\mathcal{A}}}]_{(1)(i)}^{\mathrm{T}}\right)^{\mathrm{T}}\right]^{\dagger}$;
(1.5) *From* $[\boldsymbol{\mathcal{R}}]_{(3)}$, *obtain an LS estimate of* $\boldsymbol{A}_{\mathrm{t},1}^*$:
$\hat{\boldsymbol{A}}_{\mathrm{t},1(i)}^* = [\boldsymbol{\mathcal{R}}]_{(3)} \left[\left(\boldsymbol{A}_{\mathrm{r}(i)}^* \diamond [\hat{\boldsymbol{\mathcal{A}}}]_{(1)(i)}^{\mathrm{T}}\right)^{\mathrm{T}}\right]^{\dagger}$;
(1.6) *Repeat steps (1.2)-(1.5) until convergence.*

- **Bilinear ALS Stage:**

(2.1) *Obtain* $\hat{\boldsymbol{\mathcal{A}}} \in \mathbb{C}^{P\times N\times(M-1)}$ *by reshaping the estimated 1-mode unfolding matrix* $[\hat{\boldsymbol{\mathcal{A}}}]_{(1)(i)}$ *obtained in the first stage as a third-order tensor in accordance with (17)*;
(2.2) *Set* $j = 0$ *and initialize randomly* $\hat{\boldsymbol{R}}_{\gamma(j=0)}$ *and* $\hat{\boldsymbol{A}}_{\mathrm{t},2(j=0)}$;
(2.3) $j = j + 1$;
(2.4) *From* $[\hat{\boldsymbol{\mathcal{A}}}]_{(1)}$ *and* $\hat{\boldsymbol{A}}_{\mathrm{r}(i)}$, *obtain an LS estimate of* $\boldsymbol{R}_\gamma^{\mathrm{T}}$:
$\hat{\boldsymbol{R}}_{\gamma(j)}^{\mathrm{T}} = [\hat{\boldsymbol{\mathcal{A}}}]_{(1)} \left[\left(\hat{\boldsymbol{A}}_{\mathrm{t},2(j-1)} \diamond \hat{\boldsymbol{A}}_{\mathrm{r}(i)}\right)^{\mathrm{T}}\right]^{\dagger}$;
(2.5) *From* $[\hat{\boldsymbol{\mathcal{A}}}]_{(3)}$ *and* $\hat{\boldsymbol{A}}_{\mathrm{r}(i)}$, *obtain an LS estimate of* $\boldsymbol{A}_{\mathrm{t},2}$:
$\hat{\boldsymbol{A}}_{\mathrm{t},2(j)} = [\hat{\boldsymbol{\mathcal{A}}}]_{(3)} \left[\left(\hat{\boldsymbol{A}}_{\mathrm{r}(i)} \diamond \hat{\boldsymbol{R}}_{\gamma(j)}^{\mathrm{T}}\right)^{\mathrm{T}}\right]^{\dagger}$;
(2.6) *Repeat steps (2.3)-(2.5) until convergence.*

- **DoD and DoA Parameters Estimation:**

(2.7) *From* $\hat{\boldsymbol{A}}_{\mathrm{t},1(i)}$ *and* $\hat{\boldsymbol{A}}_{\mathrm{t},2(j)}$, *obtain a final estimate of* $\hat{\boldsymbol{A}}_{\mathrm{t}}$ *using the relation (24)*;
(2.8) *From the p-th column of* $\hat{\boldsymbol{A}}_{\mathrm{t}}$ *and* $\hat{\boldsymbol{A}}_{\mathrm{r}}$, *find the estimates of* $\hat{\phi}_p$ *and* $\hat{\theta}_p$ $(p = 1, \ldots, P)$ *performing the one-dimensional peak search in the spatial spectrum (25) and (26), respectively*

Algorithm 2: Alternative closed-form solution to the second stage of the proposed algorithm.

1. *From the covariance tensor* $\boldsymbol{\mathcal{R}}$ *in (16), obtain the estimates of* $\hat{\boldsymbol{\mathcal{A}}}$, $\hat{\boldsymbol{A}}_{\mathrm{t},1}$ *and* $\hat{\boldsymbol{A}}_{\mathrm{r}}$ *using the first trilinear ALS stage in Algorithm 1;*
2. *From* $[\hat{\boldsymbol{\mathcal{A}}}]_{(2)}^{\mathrm{T}} \cdot \left(\hat{\boldsymbol{A}}_{\mathrm{r}}^{\mathrm{T}}\right)^{\dagger} = \hat{\boldsymbol{A}}_{\mathrm{t},2} \diamond \hat{\boldsymbol{R}}_\gamma^{\mathrm{T}}$, *obtain the estimates of* $\hat{\boldsymbol{A}}_{\mathrm{t},2}$ *and* $\hat{\boldsymbol{R}}_\gamma^{\mathrm{T}}$ *using the LS-KRF algorithm [34]*;
3. *From* $\hat{\boldsymbol{A}}_{\mathrm{t},1}$ *and* $\hat{\boldsymbol{A}}_{\mathrm{t},2}$, *obtain a final estimate of* $\hat{\boldsymbol{A}}_{\mathrm{t}}$ *using the relation (24)*;
4. *From the p-th column of* $\hat{\boldsymbol{A}}_{\mathrm{t}}$ *and* $\hat{\boldsymbol{A}}_{\mathrm{r}}$, *find the estimates of* $\hat{\phi}_p$ *and* $\hat{\theta}_p$ $(p = 1, \ldots, P)$ *performing the one-dimensional peak search in the spatial spectrum (25) and (26), respectively.*

5. Uniqueness issues

We assume that each factor matrix in the Nested-PARAFAC model (16) has full-rank, i.e., all targets are uncorrelated with each other and have different DoDs and DoAs. Based on this assumption, and applying Kruskal's condition [15] to the inner and outer PARAFAC tensors of the Nested-PARAFAC decomposition, we can deduce that the estimated matrices $\hat{\boldsymbol{A}}_{\mathrm{t}}$ and $\hat{\boldsymbol{A}}_{\mathrm{r}}$ are unique up to permutation and scaling of their columns if

$$\min\left(N(M-1),P\right)+\min\left(N,P\right)+\min\left(M-1,P\right)\geq 2P+2 \quad (28)$$

$$\min\left(N,P\right)+\min\left(M-1,P\right)\geq P+2. \quad (29)$$

The combination of conditions (28) and (29) yields the following two corollaries:

- If $N \geq P$, then $M \geq 3$ transmit antennas are necessary to uniquely recover the spatial parameters of P targets;
- If $M-1 \geq P$, then $N \geq 2$ receive antennas are necessary to uniquely recover the spatial parameters of P targets.

Therefore, by satisfying the conditions (28) and (29), the estimated matrices $\hat{\boldsymbol{A}}_{\mathrm{t}}$ and $\hat{\boldsymbol{A}}_{\mathrm{r}}$ satisfy the following relations:

$$\hat{\boldsymbol{A}}_{\mathrm{t}}=\boldsymbol{A}_{\mathrm{t}}\boldsymbol{\Pi}\boldsymbol{\Delta}_1+\boldsymbol{N}_1 \quad \text{and} \quad \hat{\boldsymbol{A}}_{\mathrm{r}}=\boldsymbol{A}_{\mathrm{r}}\boldsymbol{\Pi}\boldsymbol{\Delta}_2+\boldsymbol{N}_2, \quad (30)$$

where $\boldsymbol{\Pi}$ denotes a permutation matrix common for all the estimated matrices, $\boldsymbol{\Delta}_i$ $(i=1,2)$ are diagonal scaling matrices and $\boldsymbol{N}_i$ $(i=1,2)$ represent the estimation error. According (30), since $\hat{\boldsymbol{A}}_{\mathrm{t}}$ and $\hat{\boldsymbol{A}}_{\mathrm{r}}$ share the same column permutation by means of the matrix $\boldsymbol{\Pi}$, the proposed method provides automatically paired estimates of the targets' DoDs and DoAs using (25) and (26), respectively. Positioning errors can be measured as a function of the first antenna element (being the reference one), the first row of each matrix $\boldsymbol{A}_{\mathrm{t}}$ and $\boldsymbol{A}_{\mathrm{r}}$ is assumed to have unity entries. Hence, at the output of the first TALS stage, the scaling ambiguity in $\hat{\boldsymbol{A}}_{\mathrm{t},1}$ and $\hat{\boldsymbol{A}}_{\mathrm{r}}$ can be removed from this *a priori* information. By its turn, the scaling ambiguity affecting the estimate $\hat{\boldsymbol{A}}_{\mathrm{t},2}$ obtained in the second BALS stage can be removed from the second row of $\hat{\boldsymbol{A}}_{\mathrm{t},1}$ already estimated in the first stage.

6. Computational complexity

In the following, we evaluate the computational complexity of our proposed Nested-PARAFAC based estimator with respect to competing matrix-based and tensor-based algorithms proposed in the literature. The complexity of each algorithm in terms of floating point operations (flops) at each iteration is summarized in Table 1. In these expressions, the number of flops refers to the dominant costs of the algorithms, which are the computations of the SVDs required to calculate pseudo-inverses at each iteration of the iterative tensor-based algorithms. According to [35], we assume here that the computational cost to calculate the SVD of a matrix of size $I_1 \times I_2$ is $\mathcal{O}\left(I_1 \cdot I_2 \cdot \min(I_1, I_2)\right)$.

Table 1
Complexity Analysis of the Algorithms.

Algorithm	Number of float operations
2D-ESPRIT in [36]	$LNMP+2NMP^2+2P^3$
Tensor-ESPRIT in [23]	$2LNMP+2NMP^2+2P^3$
ALS-PARAFAC in [13]	$LMP^2+LNP^2+MNP^2$
ALS-Tucker4 in [24]	$2N(M-1)^2P^2+2N^2(M-1)P^2+N^2(M-1)^2P^4$
Nested-PARAFAC	
TALS (1st stage)	$N(M-1)^2P^2+N^2(M-1)P^2+N(M-1)P^2$
BALS (2nd stage)	$N(M-1)P^2+NP^3$
LS-KRF (2nd stage)	$(M-1)P^2+NP^2$

As previously mentioned, the complexity of the ALS-PARAFAC algorithm is a function of the data block size L to be processed at the receiver. In Table 1, we can see that the first two terms of the ALS-Tucker4 algorithm has double the complexity than the first two terms in the TALS stage of the Nested-PARAFAC algorithm, while the last term has quadratic complexity compared to the last term in the TALS stage. Moreover, the knowledge of $\boldsymbol{A}_{\mathrm{r}}$ in the BALS stage results in a faster convergence and lower complexity estimation, in comparison with the TALS stage. Thus, the dominant part of the complexity of the Nested-PARAFAC refers to its TALS stage. This becomes more evident when the alternative closed-form solution based on the LS-KRF algorithm is used in the second stage. Based on this analysis, we can conclude that the ALS-Tucker4 is computationally more expansive than the proposed Nested-PARAFAC algorithm. This discussion will be reinforced by the numerical results of Section 7, showing that the proposed approach yields similar performance as [13] and [24] while being more computationally attractive. Compared to the 2D-ESPRIT and Tensor-ESPRIT techniques, all the iterative tensor-based algorithms in Table 1 are computationally more expansive since the first two ones are closed-form solutions with low complexity. However, ESPRIT-based algorithms have worse performance than the tensor-based ALS-PARAFAC, ALS-Tucker4 and Nested-PARAFAC algorithms, especially in real-world scenarios in which the antenna elements at the transmit and receive arrays may be affected by calibration errors, as shown in our simulation results.

7. Simulation results

In this section, we evaluate the performance of the proposed Nested-PARAFAC estimator from computer simulations. We consider $M=6$ and $N=5$ antennas at the transmit and receive arrays, respectively. The antenna arrays are assumed to be non-uniform linear arrays (NULAs) with known positioning errors, i.e., the array manifolds are known. We assume $K=128$ samples per pulse period, a pulse duration of 5 μs, and data block of size $L=100$. Our simulated scene has three targets with Doppler frequencies $\{f_{\mathrm{D}p}\}_{p=1}^{3}=\{300,400,400\}$ Hz and reflection coefficients $\{|\beta_p|\}_{p=1}^{3}=1$, which are located at $(\phi_1,\theta_1)=(30^\circ,20^\circ)$, $(\phi_2,\theta_2)=(50^\circ,40^\circ)$ and $(\phi_3,\theta_3)=(70^\circ,60^\circ)$. Our numerical results represent an average of 1000 independent Monte Carlo runs.

In Figs. 1 and 2, we show as figures of merit the total root mean square error (RMSE) of the estimated angles as a function of the positioning error factor α for two different signal-to-noise (SNR) values (0 dB and 30 dB, respectively). The total RMSE is defined as:

$$\mathrm{RMSE}=\sqrt{E\left\{\sum_{p=1}^{P}(\phi_p-\hat{\phi}_p)^2+(\theta_p-\hat{\theta}_p)^2\right\}}, \quad (31)$$

where $\hat{\phi}_p$ and $\hat{\theta}_p$ are the estimated DoD and DoA of the p-th target, respectively. We compare the estimation accuracy of the proposed method with matrix-based 2D-ESPRIT [36], Tensor-ESPRIT [23] and the Crámer-Rao bound in [37]. We also include in our evaluation, the tensor-based competitors ALS-Tucker4 [24] and ALS-PARAFAC [13], which solve the same problem. We call attention that in the ALS-Tucker4 algorithm, the covariance matrix (14) is interpreted as a multimode unfolding of a fourth-order Tucker decomposition, and a five-step ALS-based algorithm is proposed to estimate the DoDs and DoAs of the targets from (15). The ALS-PARAFAC is a direct-data approach in which a trilinear ALS-based fitting algorithm is applied directly to received signal tensor (10), which is of size $N \times M \times L$. According to Figs. 1 and 2, the iterative ALS-based algorithms are robust to real-world scenarios with array calibration errors and have no performance degradation when

Please cite this article in press as: P.R.B. Gomes et al., A nested-PARAFAC based approach for target localization in bistatic MIMO radar systems, Digit. Signal Process. (2019), https://doi.org/10.1016/j.dsp.2019.02.005

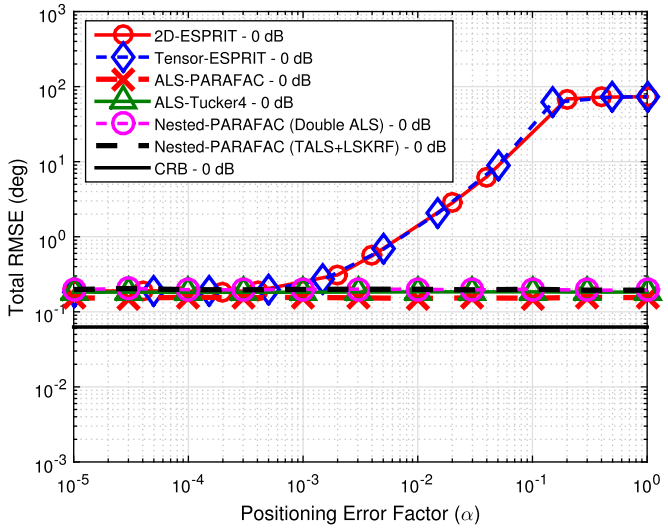

Fig. 1. Total RMSE (deg) vs. positioning error factor (α) and SNR = 0 dB.

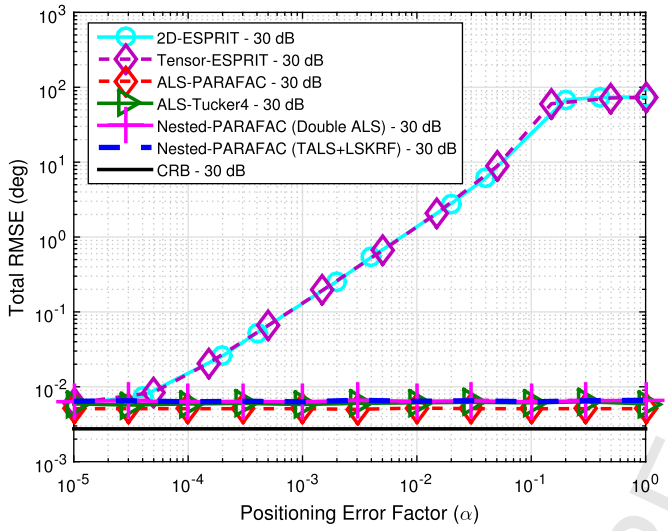

Fig. 2. Total RMSE (deg) vs. positioning error factor (α) and SNR = 30 dB.

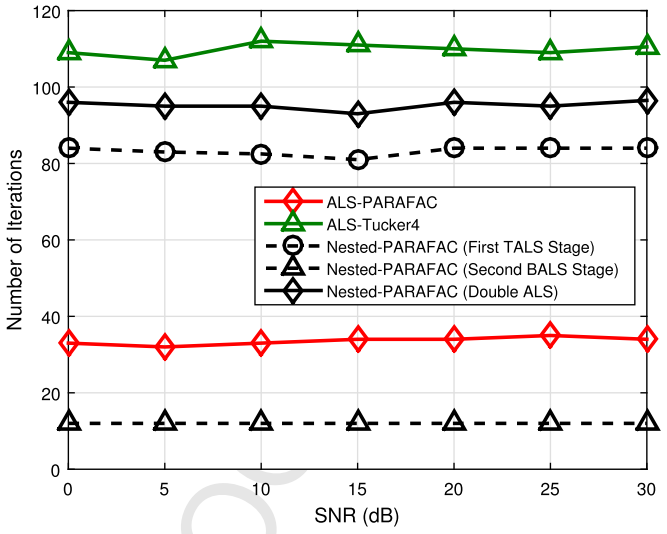

Fig. 3. Number of iterations for convergence vs. SNR (dB).

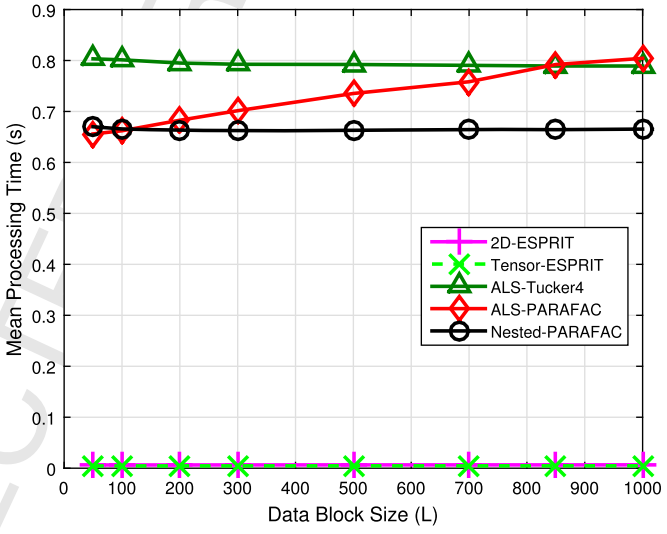

Fig. 4. Mean processing time (in seconds) vs. data block size.

the error factor α increases. On the other hand, the accuracy of matrix-based and tensor-based ESPRIT techniques is degraded due to the violation of the shift-invariance property that only holds in the ideal scenario with $\alpha \to 0$. Note that all tensor-based iterative algorithms have similar estimation accuracy. Thus, the best choice within the simulated tensor-based methods can be guided mainly by the computational complexity. This aspect is evaluated in our next experiment.

In Fig. 3, we evaluate the convergence rate of the iterative ALS-based algorithms. We plot as a figure of merit the average number of iterations required for convergence as a function of SNR in dB. In this experiment, the fast convergence of the ALS-PARAFAC algorithm does not expose its high computational cost per iteration when L is large, as shown in Table 1. Despite the same performance in terms of RMSE, the proposed Nested-PARAFAC estimator requires less iterations than the ALS-Tucker4 one. Indeed, as discussed in Section 6, most of the processing burden of the Nested-PARAFAC estimator is concentrated on its first TALS stage which corresponds to approximately 90% of the total number of iterations. Fig. 3 together with the values in Table 1 reveal that the proposed Nested-PARAFAC algorithm is preferable than the ALS-Tucker4 one in terms of computational complexity.

Fig. 4 depicts the mean processing time (in seconds) as a function of the data block size L processed at the receiver. In this experiment, we set the SNR to 30 dB. In contrast to Fig. 3, we can observe more clearly here the dependence between the computational complexity of the ALS-PARAFAC and the data block size. More specifically, for a reasonable value of L, the Nested-PARAFAC approach outperforms the ALS-PARAFAC one since the latter operates directly on the received data samples and thus has a higher computational complexity when L is large, as shown earlier in Table 1. When compared to the matrix-based 2D-ESPRIT and Tensor-ESPRIT algorithms, the Nested-PARAFAC approach has a higher computational complexity in accordance with Table 1. But the proposed method is able to operate with high accuracy in scenarios with array calibration errors, as shown in Figs. 1 and 2. These numerical results validate the merits of the proposed tensor-based approach compared to state-of-the-art matrix-based and tensor-based ones.

8. Conclusion

We have proposed a Nested-PARAFAC based method for solving the multi-target localization problem in bistatic MIMO radar systems without imposing constraints on the geometry in the trans-

Please cite this article in press as: P.R.B. Gomes et al., A nested-PARAFAC based approach for target localization in bistatic MIMO radar systems, Digit. Signal Process. (2019), https://doi.org/10.1016/j.dsp.2019.02.005

mit and receive arrays. The proposed Nested-PARAFAC estimator offers the same performance as that of competing methods [13] and [24], while being less computationally complex. At the same time, our solution is robust to positioning errors of the antennas, in contrast to competing 2D-ESPRIT and Tensor-ESPRIT techniques.

Conflict of interest statement

The authors declare that there is no conflict of interests regarding the publication of this paper.

Acknowledgments

This work has been supported by the National Council for Scientific and Technological Development – CNPq, CAPES/PROBRAL Processo no. 88887.144009/2017-00, and FUNCAP.

References

[1] Z. Zheng, J. Zhang, J. Zhang, Joint DoD and DoA estimation for bistatic MIMO radar in the presence of unknown mutual coupling, Signal Process. 92 (Jun. 2012) 3039–3048.
[2] C. Gu, J. He, H. Li, X. Zhu, Target localization using MIMO electromagnetic vector array systems, Signal Process. 93 (Feb. 2013) 2103–2107.
[3] H. Jiang, Y. Zhang, J. Li, H. Cui, PARAFAC-based algorithm for multidimensional parameter estimation in polarimetric bistatic MIMO radar, EURASIP J. Adv. Signal Process. 2013 (2013) 133.
[4] X. Wang, W. Wang, X. Li, J. Wang, A tensor-based subspace approach for bistatic MIMO radar in spatial colored noise, Sensors 14 (2014) 3897–3907.
[5] A.M. Haimovich, R. Blum, L. Cimini, MIMO radar with widely separated antennas, IEEE Signal Process. Mag. 25 (1) (Jan. 2008) 116–129.
[6] J. Li, P. Stoica, MIMO radar with colocated antennas, IEEE Signal Process. Mag. 24 (5) (Sep. 2007) 106–114.
[7] J. Tan, Z. Nie, D. Wen, Low complexity MUSIC-based direction-of-arrival algorithm for monostatic MIMO radar, Electron. Lett. 53 (4) (Feb. 2017) 275–277.
[8] X.L. Liu, G.S. Liao, Multi-target localisation in bistatic MIMO radar, Electron. Lett. 46 (13) (Jun. 2010) 945–946.
[9] R. Xie, Z. Liu, J. Wu, Direction finding with automatic pairing for bistatic MIMO radar, Signal Process. 92 (Jul. 2011) 198–203.
[10] J. Li, X. Zhang, R. Cao, M. Zhou, Reduced-dimension MUSIC for angle and array gain-phase error estimation in bistatic MIMO radar, IEEE Commun. Lett. 17 (3) (Mar. 2013) 443–446.
[11] J. Chen, H. Gu, W. Su, A new method for joint DoD and DoA estimation in bistatic MIMO radar, Signal Process. 90 (Aug. 2010) 714–718.
[12] M. Jin, G. Liao, J. Li, Joint DoD and DoA estimation for bistatic MIMO radar, Signal Process. 89 (Aug. 2009) 244–251.
[13] D. Nion, N.D. Sidiropoulos, Tensor algebra and multidimensional harmonic retrieval in signal processing for MIMO radar, IEEE Trans. Signal Process. 58 (11) (Nov. 2010) 5693–5705.
[14] J.D. Carroll, J. Chang, Analysis of individual differences in multi-dimensional scaling via an n-way generalization of Eckart-Young decomposition, Psychometrika 35 (3) (1970) 283–319.
[15] R.A. Harshman, Foundations of the PARAFAC procedure: model and conditions for an explanatory multi-mode factor analysis, UCLA Work. Pap. Phon. 16 (1) (1970) 1–84.
[16] H.Y. Zhao, Z.J. Zhang, J. Liu, S. Zhou, J. Zheng, W. Liu, Target detection based on F-test in passive multistatic radar, Digit. Signal Process. 79 (2018) 1–8.
[17] J. Liu, W. Zhou, X. Wang, D. Huang, A sparse direction-of-arrival estimation algorithm for MIMO radar in the presence of gain-phase errors, Digit. Signal Process. 69 (2017) 193–203.
[18] S. Qin, Y.D. Zhang, M.G. Amin, DOA estimation of mixed coherent and uncorrelated targets exploiting coprime MIMO radar, Digit. Signal Process. 61 (2017) 26–34.
[19] F. Wen, X. Xiong, Z. Zhang, Angle and mutual coupling estimation in bistatic MIMO radar based on PARAFAC decomposition, Digit. Signal Process. 65 (2017) 1–10.
[20] A.L.F. de Almeida, G. Favier, Double Khatri-Rao space-time-frequency coding using semi-blind PARAFAC based receiver, IEEE Signal Process. Lett. 20 (5) (May. 2013) 471–474.
[21] K. Liu, J.P.C.L. da Costa, H.C. So, A.L.F. de Almeida, Semi-blind receivers for joint symbol and channel estimation in space-time-frequency MIMO-OFDM systems, IEEE Trans. Signal Process. 61 (21) (Nov. 2013) 5444–5457.
[22] R. Roy, T. Kailath, ESPRIT-estimation of signal parameters via rotational invariance techniques, IEEE Trans. Acoust. Speech Signal Process. 37 (7) (Jul. 1989) 984–995.
[23] M. Haardt, F. Roemer, G. del Galdo, Higher-order SVD-based subspace estimation to improve the parameter estimation accuracy in multidimensional harmonic retrieval problems, IEEE Trans. Signal Process. 56 (7) (Jul. 2008) 3198–3213.
[24] P.R.B. Gomes, A.L.F. de Almeida, J.P.C.L. da Costa, G. del Galdo, Tensor-based methods for blind spatial signature estimation under arbitrary and unknown source covariance structure, Digit. Signal Process. 62 (Mar. 2017) 197–210.
[25] L.R. Ximenes, G. Favier, A.L.F. de Almeida, Semi-blind receivers for non-regenerative cooperative MIMO communications based on nested PARAFAC modeling, IEEE Trans. Signal Process. 63 (18) (Sep. 2015) 4985–4998.
[26] L.R. Ximenes, G. Favier, A.L.F. de Almeida, Closed-form semi-blind receiver for MIMO relay systems using double Khatri-Rao space-time coding, IEEE Signal Process. Lett. 23 (3) (Mar. 2016) 316–320.
[27] W.C.F. Júnior, G. Favier, A.L.F. de Almeida, Sequential closed-form semiblind receiver for space-time coded multihop relaying systems, IEEE Signal Process. Lett. 24 (12) (Dec. 2017) 1773–1777.
[28] T.G. Kolda, B.W. Bader, Tensor decompositions and applications, SIAM Rev. 51 (3) (Aug. 2009) 455–500.
[29] A. Cichocki, D.P. Mandic, A.H. Phan, C.F. Caiafa, G. Zhou, Q. Zhao, L. De Lathauwer, Tensor decompositions for signal processing applications from two-way to multiway component analysis, IEEE Signal Process. Mag. 32 (2) (2015) 145–163.
[30] J.P.C.L. da Costa, F. Roemer, M. Haardt, R.T. de Sousa Jr., Multi-dimensional model order selection, EURASIP J. Adv. Signal Process. 26 (20) (Jul. 2011), Springer publisher.
[31] K. Liu, J.P.C.L. da Costa, C. So, L. Huang, J. Ye, Detection of number of components in CANDECOMP/PARAFAC models via minimum description length, Digit. Signal Process. 51 (2016) 110–123.
[32] R. Bro, Multi-Way Analysis in the Food Industry: Models, Algorithms and Applications, Ph.D. dissertation, University of Amsterdam, Amsterdam, 1998.
[33] J.P.C.L. da Costa, F. Roemer, M. Weis, M. Haardt, Robust R-D parameter estimation via closed-form PARAFAC, in: Proc. ITG Workshop on Smart Antennas, WSA'10, Bremen, Germany, 2010.
[34] F. Roemer, M. Haardt, Tensor-based channel estimation and iterative refinements for two-way relaying with multiple antennas and spatial reuse, IEEE Trans. Signal Process. 58 (11) (Nov. 2010) 5720–5735.
[35] G.H. Golub, C.F. Van Loan, Matrix Computations, Johns Hopkins University Press, Baltimore, MS, USA, 1996.
[36] J. Chen, H. Gu, W. Su, Angle estimation using ESPRIT without pairing in MIMO radar, Electron. Lett. 44 (24) (Nov. 2008) 1422–1423.
[37] F. Roemer, M. Haardt, A framework for the analytical performance assessment of matrix and tensor-based ESPRIT-type algorithms, CoRR, arXiv:1209.3253, url http://arxiv.org/abs/1209.3253, 2012.

Paulo R. B. Gomes received the Diploma degrees in physics in 2011 from the Federal University of Ceará (UFC) and telecommunications engineering in 2014 from the Federal Institute of Education, Science and Technology of Ceará (IFCE), both in Ceará, Brazil, his M.Sc (in 2014) and Ph.D. (in 2018) degrees in teleinformatics engineering also from the UFC. His research interests are on tensor-based signal processing techniques with applications to sensors arrays, radar and wireless communication systems.

André L. F. de Almeida is an Associate Professor with the Department of Teleinformatics Engineering of the Federal University of Ceará. He has over 50 refereed journal articles published and accepted, 100 conference papers and 5 book chapters. He served as an Associate Editor for the IEEE Transactions on Signal Processing (2012-2016). He currently serves as an Associate Editor for the IEEE Signal Processing Letters. His current research has a focus on: (i) tensor-based blind/semi-blind techniques; (ii) and collaborative distributed estimation for networks and (iii) multilinear algebra with application to signal processing and data analytics.

João Paulo C. L. da Costa received the Diploma degree in electronic engineering in 2003 from the Military Institute of Engineering (IME), Rio de Janeiro, Brazil, his M.Sc. degree in telecommunications in 2006 from University of Brasilia (UnB), Brazil, and his Ph.D. degree in electrical and information engineering in 2010 at TU Ilmenau, Germany. Since 2010, he coordinates the Laboratory of Array Signal Processing (LASP). From 2014 to 2017, he coordinated a special visiting researcher (PVE) project related to satellite navigation with the German Aerospace Center (DLR) supported by CAPES and CNPq, and since 2014, he is a project coordinator in a distance learning project at the National School of Public Administration (Enap).

Rafael T. de Sousa Jr. was born in Campina Grande - PB, Brazil, on june 24, 1961. He graduated in Electrical Engineering from the Federal Uni-

versity of Paraíba (UFPB), Campina Grande - PB, Brazil, 1984, and got his Doctorate Degree in Telecommunications from the University of Rennes 1, Rennes, France, 1988. He worked as a software and network engineer in the private sector from 1989 to 1996. Since 1996, he is a Network Engineering Professor in the Electrical Engineering Department, at the University of Brasília, Brazil. From 2006 to 2007, supported by the Brazilian R&D Agency CNPq, He took a sabbatical year in the Group for the Security of Information Systems and Networks, at Ecole Superiéure d'Electricité, Rennes, France. He is a member of the Post-Graduate Program on Electrical Engineering (PPGEE) and supervises the Decision Technologies Laboratory (LATITUDE) of the University of Brasília. His field of study is distributed systems and network management and security.

Please cite this article in press as: P.R.B. Gomes et al., A nested-PARAFAC based approach for target localization in bistatic MIMO radar systems, Digit. Signal Process. (2019), https://doi.org/10.1016/j.dsp.2019.02.005